

Electronic Supplementary Information

***In situ* exsolved Co components on wood ear-derived porous carbon for catalyzing oxygen reduction over a wide pH range**

Yu Xu,[‡] Haiyan Zhang,[‡] Ping Zhang, Min Lu,^{*} Xiaoji Xie^{*} and Ling Huang

Key Laboratory of Flexible Electronics (KLOFE), Institute of Advanced Materials (IAM), Nanjing Tech University (NanjingTech), Nanjing 211816, P. R. China

E-mail: iammlv@njtech.edu.cn; iamxjie@njtech.edu.cn

Experimental Details

Materials

The dry wood ear (Tianqu brand) was purchased from the local supermarket. ZnCl₂ (≥ 98%) was purchased from Shanghai Xinbao Fine Chemicals. CoCl₂ (AR) was purchased from Guangzhou Chemical Reagent Factory. H₂SO₄ (AR), KOH (≥ 99.5%), HCl (AR), NH₃·H₂O (AR), KCl (AR), and Na₂HPO₄ (AR) were purchased from Shanghai Lingfeng Chemicals. NaSCN (AR) and CH₃OH (SR) were purchased from Admas-beta. NH₄Cl (AR) and NaH₂PO₄ (AR) were purchased from Xilong Chemicals. Zn(CH₃COO)₂ (AR) was purchased from Shanghai Aladdin Reagent Co., Ltd. 20% Pt/C catalyst (Johnson Matthey), 70% PtRu/C catalyst (Johnson Matthey), 5% Nafion solution (Dupont), and Nafion 117 membrane (Dupont) were purchased from Shanghai Hesun Electric Co., Ltd. All chemicals were used as received unless otherwise noted.

Characterizations

Thermogravimetric (TG) analysis of wood ears was performed on a TG analyzer (TGA 2, Mattler-Toledo) in the N₂ atmosphere with a ramp rate of 10 °C min⁻¹. X-ray diffraction (XRD) analysis was carried out on a Rigaku Smartlab (9 kW) X-ray diffractometer equipped with a Cu K α radiation ($\lambda = 1.5406 \text{ \AA}$). The N₂-sorption isotherms and BET (Brunauer-Emmett-Teller) surface area of the

catalysts were analyzed using a surface area and porosity analyzer (ASAP 2460, Micromeritics) at 77 K. Scanning electron microscopy (SEM) images and energy dispersive spectra were obtained on a scanning electron microscope (SU 8220, Hitachi) equipped with an energy dispersive spectrometer (Emax, Horiba). Raman spectra were collected on a confocal microscope-Raman spectrometer (LabRAM HR Evolution, Horiba). Organic elemental content was analyzed on an organic elemental analyzer (Vario EL Cube, Elementar). Inductively coupled plasma mass spectrometry (ICP-MS) was carried out on the iCAP Qc (Thermo Scientific, USA) to measure the content of Co element. X-ray photoelectron spectroscopy (XPS) analysis was carried out on a ESCALAB 250Xi spectrometer (Thermo Scientific, USA) equipped with a pass energy of 30 eV with a power of 100 W (10 kV and 10 mA) and a mono-chromatized AlK α X-ray ($h\nu = 1486.65$ eV) source. The electrochemical tests were carried out on an electrochemical workstation (Zennium, Zahner) using a rotating ring-disk electrode (E7R9 (Tip), Shaft (MSR), Pine Research Instrumentation).

Electrochemical tests

To test the performance of obtained catalysts, 5 mg of the Co-C catalyst were first added into a mixture of deionized water (750 μ L), isopropanol (250 μ L), and 5% Nafion solution (16 μ L). The resulting mixture was ultrasonicated for 30 min to form a uniform catalyst ink. 60 μ L of the ink were then drop-casted onto the polished glassy carbon disk (diameter: 5.5 mm) of the rotating ring-disk electrode under a steady rotation (700 rpm) to load the Co-C catalyst with 1.2 mg cm⁻². For comparison, the 20% Pt/C catalyst was coated onto the glassy carbon disk to yield a loading of 0.2 mg cm⁻² using the same drop-casting method. The electrochemical tests were carried out using the catalyst-coated electrode as the working electrode in a certain electrolyte. The alkaline electrolyte was a KOH solution (0.1 M), the neutral electrolyte was the phosphate buffer (50 mM, a solution of 31.3 mM Na₂HPO₄ and 18.7 mM NaH₂PO₄, pH = 7), and the acidic electrolyte was a H₂SO₄ solution (0.5 M). Notably, the Ag/AgCl/KCl (3 M) electrode was used as the reference electrode, and the potential was converted into the reversible hydrogen electrode (RHE) scale using Equation S1 for the comparison of ORR activities in different electrolytes.

$$E_{RHE} = E_{Ag/AgCl} + 0.214 + 0.059 \times \text{pH} \quad (\text{S1})$$

Prior to electrochemical tests, the electrolyte was pre-purged with N₂ or O₂ for 30 min to create a N₂-saturated or O₂-saturated environment, respectively. Cyclic voltammetry (CV) was tested at a scan rate of 50 mV s⁻¹ in static conditions. Linear sweep voltammetry (LSV) was tested at a rate of 5 mV s⁻¹ with rotating rates from 625 rpm to 2500 rpm. The current of the glassy carbon disk was

recorded against the changing potential. According to Koutecky-Levich Equation (Equation S2), $1/j$ is plotted against $\omega^{-1/2}$.

$$\frac{1}{j} = \frac{1}{j_L} + \frac{1}{j_K} = \frac{1}{B\omega^{1/2}} + \frac{1}{j_K} \quad (\text{S2})$$

where j is the current density of the glassy carbon disk, j_L and j_K are the limiting and kinetic current densities, respectively, ω is the rotation rate (rpm) of the disk, and B is defined by Equation S3.

$$B = 0.2nFC_0(D_0)^{2/3}\nu^{-1/6} \quad (\text{S3})$$

where n is the electron transfer number, F is the Faraday constant (96485 C mol^{-1}), C_0 is the bulk concentration of O_2 ($1.2 \times 10^{-6} \text{ mol cm}^{-3}$), D_0 is the diffusion coefficient of O_2 ($1.9 \times 10^{-5} \text{ cm}^2 \text{ s}^{-1}$), and ν is the kinematic viscosity of the electrolyte ($0.01 \text{ cm}^2 \text{ s}^{-1}$).

For the rotating ring-disk electrode (RRDE) test, the disk current density (j_d) and ring current density (j_r) were recorded simultaneously, using a scan rate of 5 mV s^{-1} , a rotating rate of 1600 rpm, and a ring potential of 1.50 V vs. RHE. The H_2O_2 selectivity and electron transfer number were obtained using the following equations (Equation S4 and S5).

$$\text{H}_2\text{O}_2\% = 200 \times \frac{j_r/N}{j_d + j_r/N} \quad (\text{S4})$$

$$n = 4 \times \frac{j_d}{j_r/N + j_d} \quad (\text{S5})$$

where j_d is the disk current density, j_r is the ring current density, N is current collection efficiency of Pt ring (38%, empirically determined using the ferrocyanide/ferricyanide redox system), and n is the electron transfer number.

For the accelerated durability test (ADT), the linear sweep voltammetry was at first measured in O_2 -saturated electrolytes at a rate of 5 mV s^{-1} , and measured again after 5000 cycles of scan (100 mV s^{-1}) for comparison. In the KOH solution (0.1 M), the cyclic scan was carried out in the potential range of 0.1 to -0.3 V (vs. Ag/AgCl/KCl (3 M)). In the phosphate buffer (50 mM), the cyclic scan was carried out in the potential range of 0.2 to -0.2 V (vs. Ag/AgCl/KCl (3 M)).

The electrochemically active surface area (ECSA) of all catalysts was obtained according to Equation S6.

$$\text{ECSA} = R_f \times S \quad (\text{S6})$$

where S is generally equal to the geometric area of the working electrode, and R_f is the roughness factor. Meanwhile, the value of R_f was determined by Equation S7.

$$R_f = C_{dl}/S/C_s \quad (S7)$$

where C_{dl} is the double-layer capacitance, and C_s is $40 \mu\text{F cm}^{-2}$. C_{dl} was estimated by plotting the current (i) at various scan rates from 5 to 50 mV s^{-1} in the non-Faradaic zone (open circuit potential $\pm 0.05 \text{ V}$) in 0.1 M KOH solution. The specific activity was obtained by normalizing the current to ECSA.

The turnover frequency (TOF, s^{-1}) can be derived using Equation S8.

$$TOF = i/(4 \times F \times n) \quad (S8)$$

where i is the current (A) in the linear sweep voltammogram, F is the Faraday's constant ($96485.3 \text{ C mol}^{-1}$), n is the number of active sites (mol, by assuming Co as the active sites). The factor of 4 is based on the consideration that four electrons are needed to produce one oxygen molecule.

Fuel cell tests

The Co-C-16 and Co-C-0 catalysts as well as the benchmark Pt/C catalyst were tested in an alkaline Zn-air fuel cell, neutral Zn-air fuel cell, half-cell, and direct methanol fuel cell.

The Zn-air fuel cell was assembled in a cubic configuration (Figure S11a). A Zn plate (4.5 cm^2 , thickness: 0.2 mm) was used as the anode. A carbon cloth (1 cm^2), coated with polytetrafluoroethylene (13.5 mg cm^{-2}) on the air-facing side and catalysts (Co-C: 1.2 mg cm^{-2} or Pt/C: 0.2 mg cm^{-2}) on the electrolyte-facing side, was used as the cathode. The distance between the anode and cathode was 1.4 cm , and the volume of electrolyte was 4 mL . For the alkaline Zn-air fuel cell, the electrolyte was a solution containing KOH (6 M) and $\text{Zn}(\text{CH}_3\text{COO})_2$ (0.2 M). For the neutral Zn-air fuel cell, the electrolyte was a solution containing NH_4Cl (4.0 M) and KCl (2.0 M), and the pH of the electrolyte was adjusted to 7 by $\text{NH}_3 \cdot \text{H}_2\text{O}$. The polarization curve was measured by LSV at a scan rate of 5 mV s^{-1} .

The half-cell was assembled using a three electrode system as shown in Figure S12. A carbon cloth (9 cm^2), coated with polytetrafluoroethylene (13.5 mg cm^{-2}) on the air-facing side and catalysts (Co-C: 1.2 mg cm^{-2} or Pt/C: 0.2 mg cm^{-2}) on the electrolyte-facing side, was used as the working electrode. An Ag/AgCl/KCl (3 M) electrode was used as the reference electrode. A Pt mesh was used as the counter electrode. The electrolyte was the phosphate buffer (30 mL, pH = 7)

containing Na_2HPO_4 (31.3 mM) and NaH_2PO_4 (18.7 mM). The polarization curve was measured by LSV at a scan rate of 5 mV s^{-1} .

The direct methanol fuel cell (DMFC) was assembled using an H-type reactor (Figure S11b). A carbon plate (2 cm^2) coated with 70% PtRu/C (2 mg cm^{-2}) was used as the anode. Another carbon plate (2 cm^2), coated with catalysts (Co-C: 1.2 mg cm^{-2} or Pt/C: 0.2 mg cm^{-2}) was used as the cathode. The anolyte was a solution of H_2SO_4 (0.5 M) and CH_3OH (1 M), and the catholyte was a solution of H_2SO_4 (0.5 M). A proton exchange membrane (Nafion 117) was placed in between to separate the anolyte and catholyte, and both electrodes were immersed in the electrolytes. Before the polarization curve was measured, the DMFC was activated by cyclic voltammetry, with a scan rate of 0.1 V s^{-1} for 40 cycles, at the potential window of 1.0 to -0.2 V (vs. Ag/AgCl/KCl (3 M)). The polarization curve was measured by LSV from the open circuit voltage to 0.3 V at a scan rate of 10 mV s^{-1} .

Figures and Tables

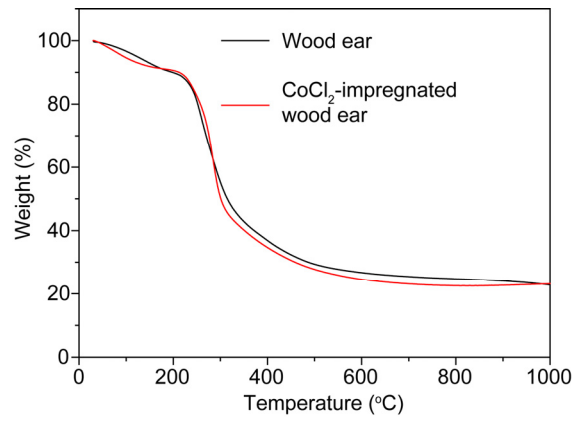


Figure S1. TG curves of the dry wood ear with and without CoCl₂ impregnation.

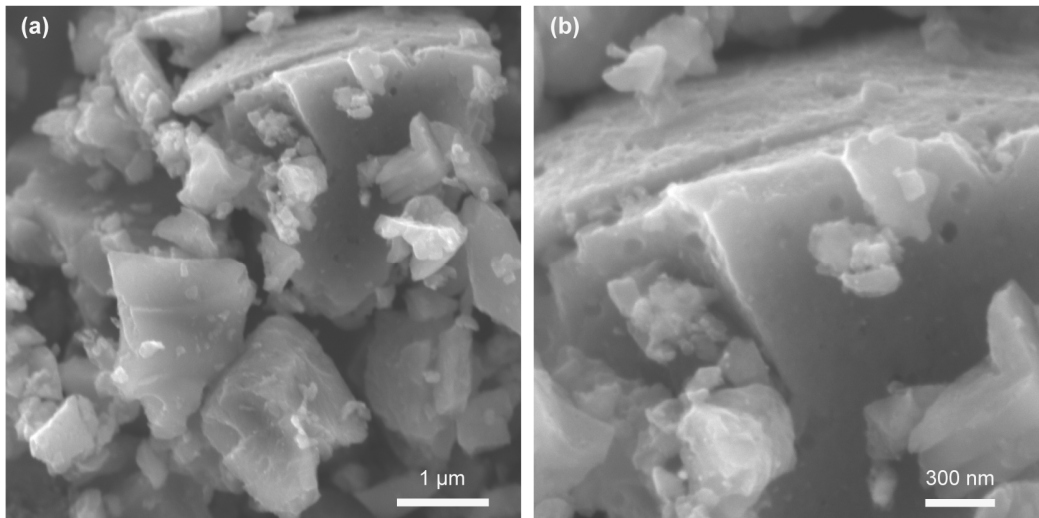


Figure S2. SEM images of the Co-C-0 catalyst at different scales.

Table S1. Element contents in Co-C catalysts.

Catalyst	C (wt%) ^a	H (wt%) ^a	N (wt%) ^a	S (wt%) ^a	Co (wt%) ^b
Co-C-0	81.81	2.62	1.75	0.14	-
Co-C-16	77.20	0.78	0.66	0.14	0.61

^a determined by organic element analysis. ^b determined by ICP-MS.

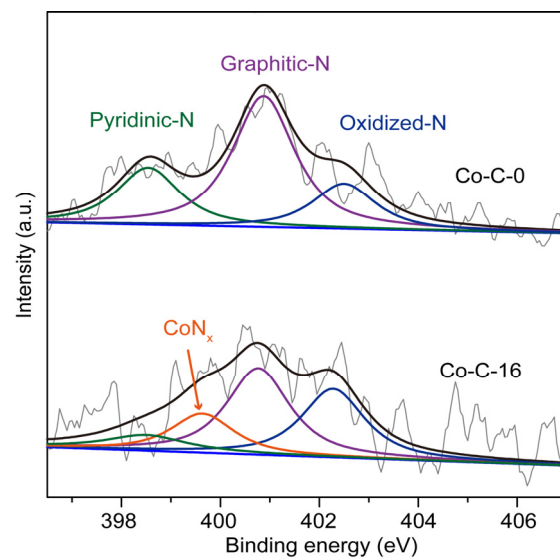


Figure S3. High-resolution N 1s XPS spectra of Co-C-0 and Co-C-16 catalysts.

Table S2. Electrochemical performance of catalysts for ORR in O₂-saturated electrolytes.^a

Catalyst	KOH (0.1 M)			PB (50 mM) ^d			H ₂ SO ₄ (0.5 M)		
	E_{onset}^b	$E_{1/2}$	j_{lim}^c	E_{onset}^b	$E_{1/2}$	j_{lim}^c	E_{onset}^b	$E_{1/2}$	j_{lim}^c
Co-C-16	0.917	0.855	4.75	0.715	0.630	3.10	0.799	0.666	2.79
Co-C-0	0.909	0.859	4.26	0.678	0.532	2.98	0.754	0.658	2.87
Pt/C	0.916	0.859	4.99	0.806	0.672	5.09	0.868	0.837	4.49

^a The unit of E_{onset} and $E_{1/2}$ is V and the unit of j_{lim} is mA cm⁻².

^b E_{onset} is defined as the potential at the current of 1 mA cm⁻².

^c j_{lim} is the sum of two distances. One is the distance between the mid-point of the voltammogram and the current baseline. The other is the distance between the mid-point of the voltammogram and the extrapolated line of the current in the mass-transfer zone.

^d PB: phosphate buffer.

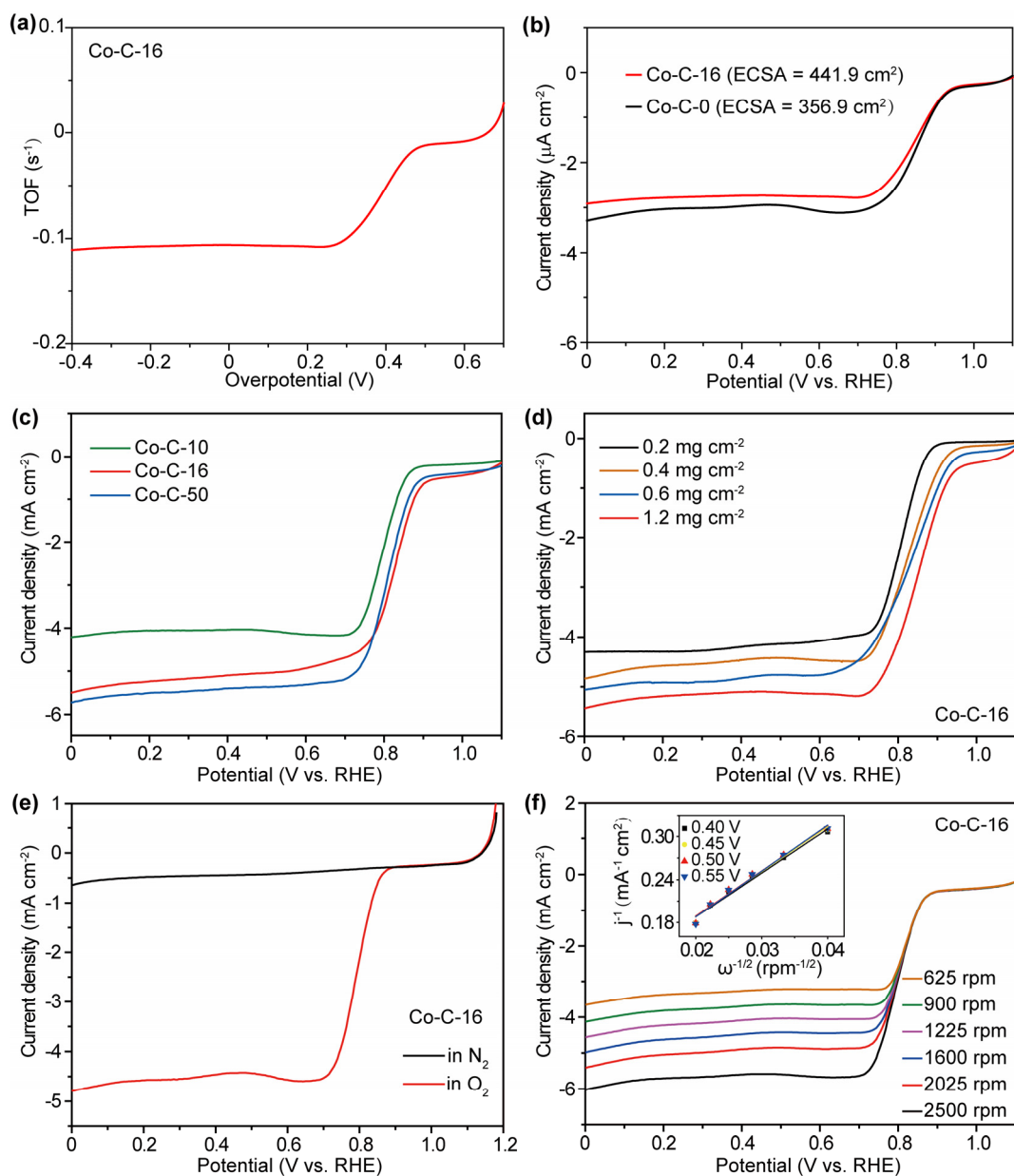


Figure S4. (a) TOF value of the Co-C-16 catalyst in a KOH (0.1 M) solution. (b) The specific activity of Co-C-0 and Co-C-16 catalysts in a KOH (0.1 M) solution. (c) Linear sweep voltammograms of Co-C-x catalysts ($x = 10, 16, 50$) in the O_2 -saturated KOH (0.1 M) solution at a rotating rate of 1600 rpm. (d) Linear sweep voltammograms of the Co-C-16 catalyst with different loading amounts at a rotating rate of 1600 rpm in the O_2 -saturated KOH (0.1 M) solution. (e) Linear sweep voltammograms of the Co-C-16 catalyst in both N_2 and O_2 -saturated KOH (0.1 M) solutions at a rotating rate of 1600 rpm. (f) Linear sweep voltammograms of the Co-C-16 catalyst at different

rotating rates in the O₂-saturated KOH (0.1 M) solution. The inset in (f) shows the corresponding K-L plots.

In Figure S4d, a reducing current appeared in the potential range of 0.94 to 1.10 V, and the reducing current increased with the increase of catalyst loading. Meanwhile, in the N₂-saturated KOH (0.1 M) solution, a similar reducing current was also observed in the voltammograms (Figure S4e). Consequently, we deduced the reducing current as the non-faradaic capacitive current ascribed to the porous carbon structure, and we subtracted it for calculating j_{lim} unless otherwise noted.

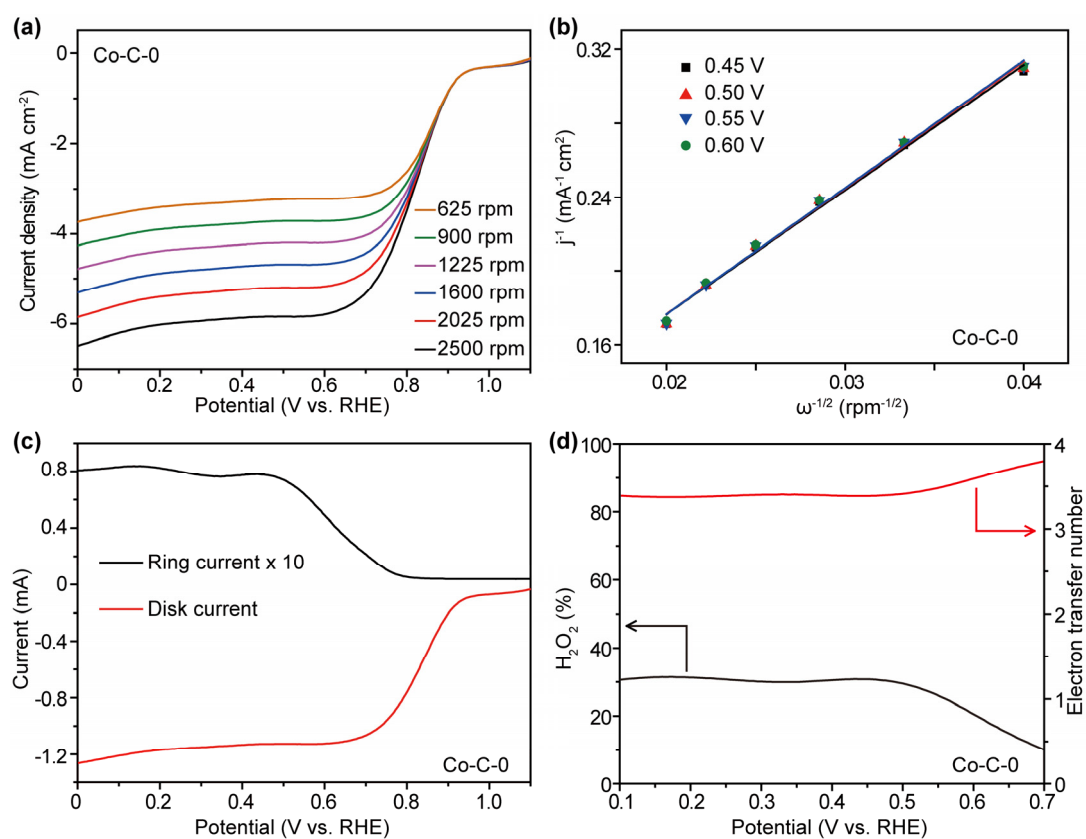


Figure S5. (a) Linear sweep voltammograms of the Co-C-0 catalyst at different rotating rates in the O₂-saturated KOH (0.1 M) solution, and (b) corresponding K-L plots. (c) Ring and disk currents on a rotating ring-disk electrode using the Co-C-0 catalyst in the O₂-saturated KOH (0.1 M) solution at a rotating rate of 1600 rpm, and (d) corresponding peroxide yields and electron transfer numbers.

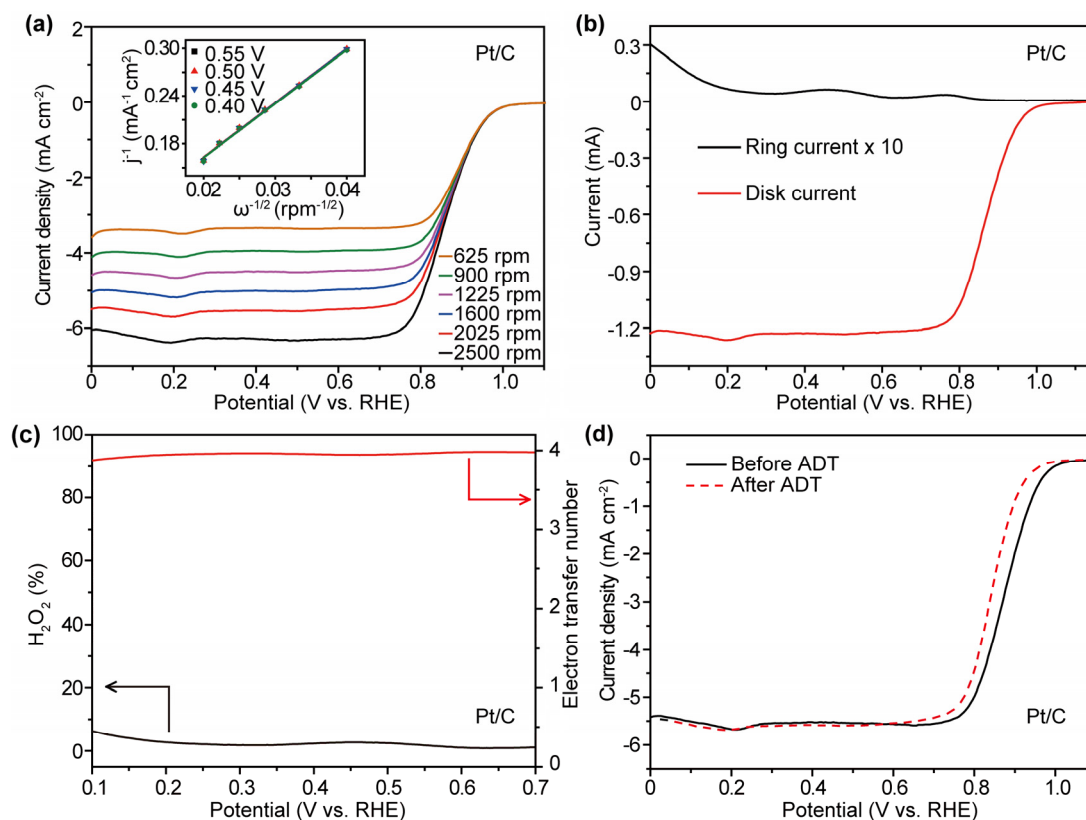


Figure S6. (a) Linear sweep voltammograms of the Pt/C catalyst at different rotating rates in the O₂-saturated KOH (0.1 M) solution. The inset shows corresponding K-L plots. (b) Ring and disk currents on a rotating ring-disk electrode using the Pt/C catalyst in the O₂-saturated KOH (0.1 M) solution at a rotating rate of 1600 rpm, and (c) corresponding peroxide yields and electron transfer numbers. (d) Linear sweep voltammograms of the Pt/C catalyst before and after 5000 cycles of the accelerated durability test (ADT) at a rotating rate of 1600 rpm.

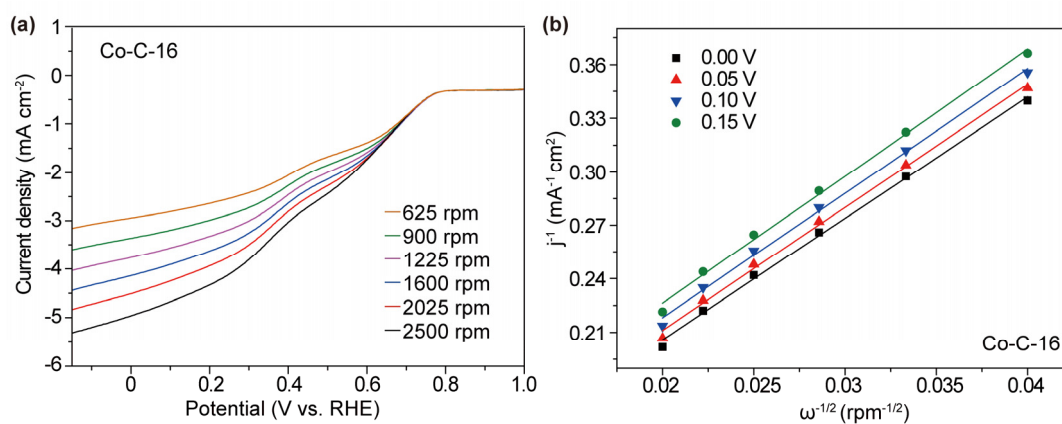


Figure S7. (a) Linear sweep voltammograms of the Co-C-16 catalyst at different rotating rates in the O_2 -saturated phosphate buffer (50 mM, pH = 7), and (b) corresponding K-L plots.

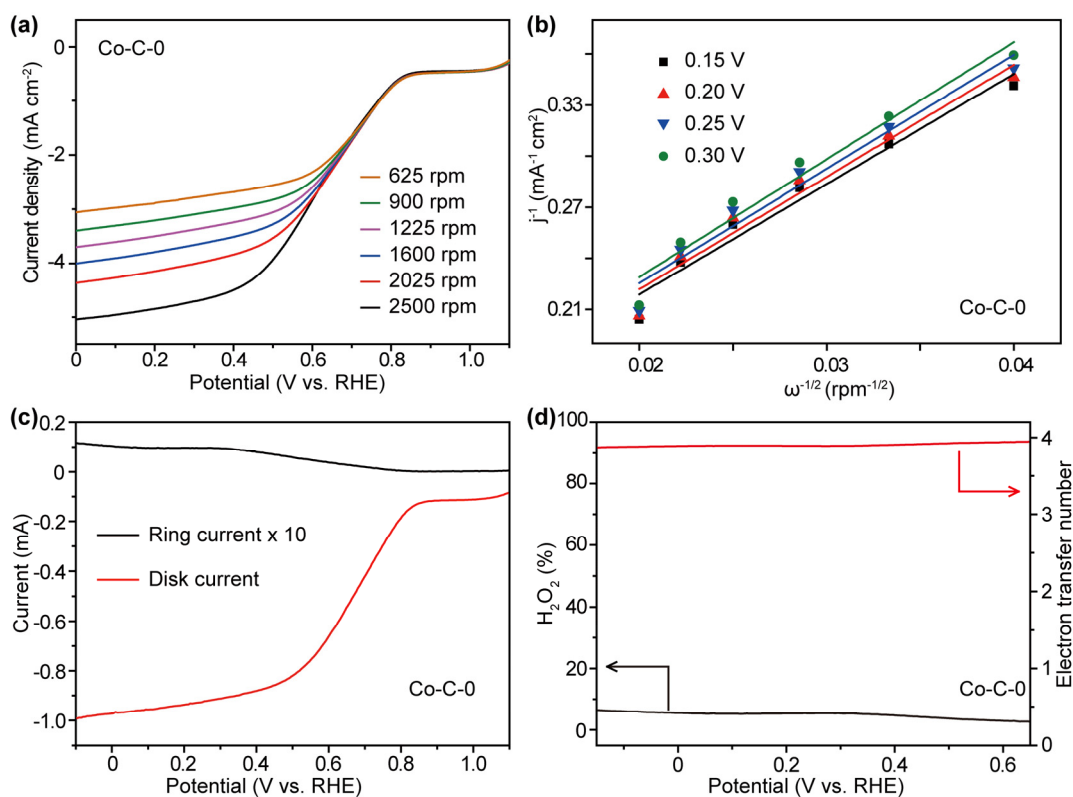


Figure S8. (a) Linear sweep voltammograms of the Co-C-0 catalyst at different rotating rates in the O₂-saturated phosphate buffer (50 mM, pH = 7), and (b) corresponding K-L plots. (c) Ring and disk currents on a rotating ring-disk electrode using the Co-C-0 catalyst in the O₂-saturated phosphate buffer (50 mM) at a rotating rate of 1600 rpm, and (d) corresponding peroxide yields and electron transfer numbers.

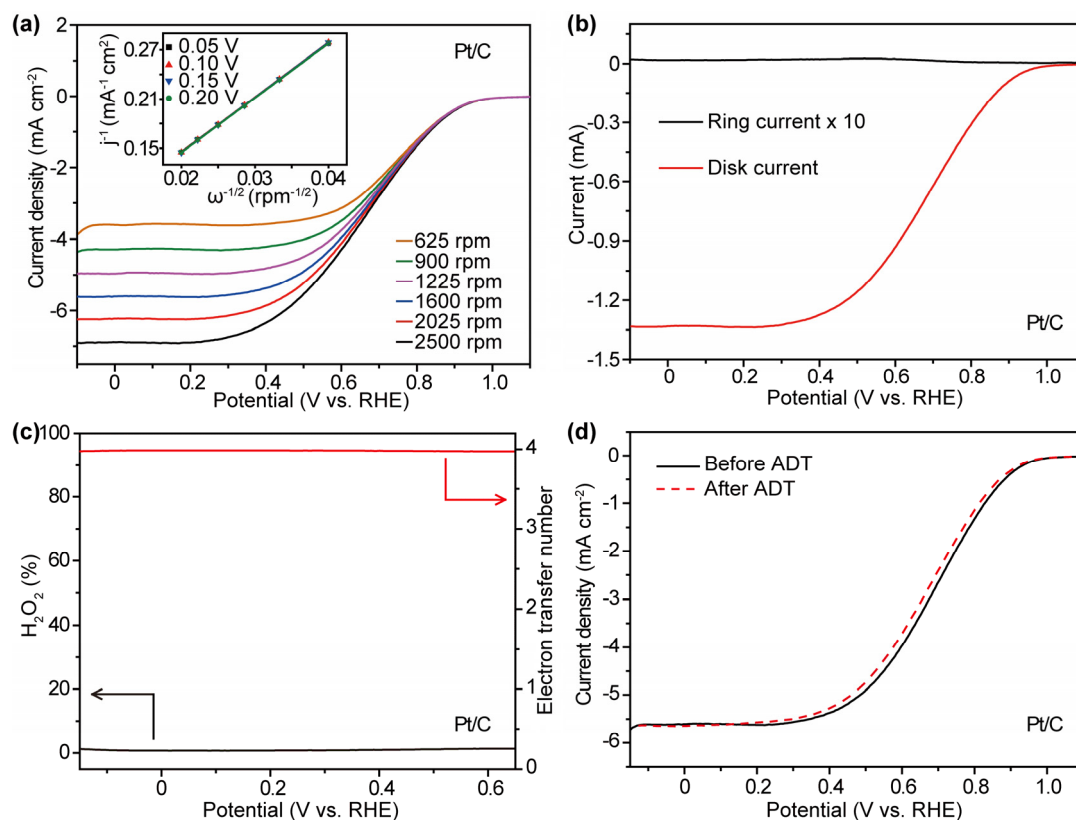


Figure S9. (a) Linear sweep voltammograms of the Pt/C catalyst at different rotating rates in the O₂-saturated phosphate buffer (50 mM, pH = 7). The inset shows corresponding K-L plots. (b) Ring and disk currents on a rotating ring-disk electrode using the Pt/C catalyst in the O₂-saturated phosphate buffer (50 mM) at a rotating rate of 1600 rpm, and (c) corresponding peroxide yields and electron transfer numbers. (d) Linear sweep voltammograms of the Pt/C catalyst before and after 5000 cycles of the accelerated durability test (ADT) at a rotating rate of 1600 rpm.

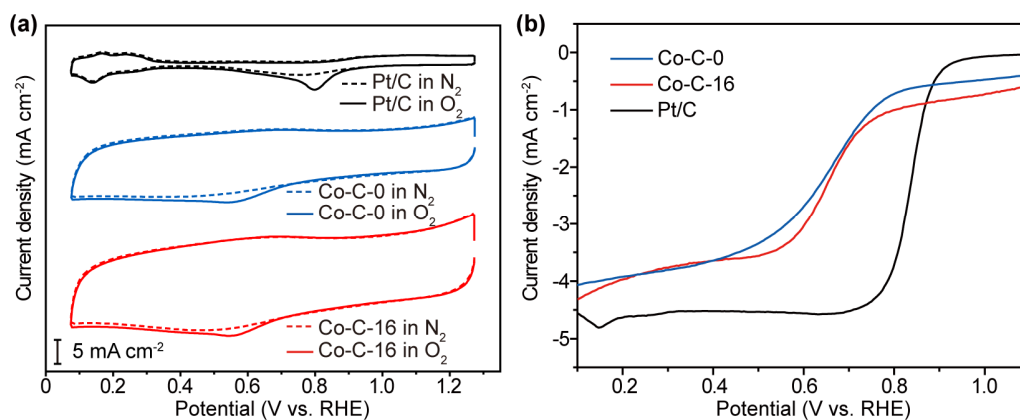


Figure S10. (a) Cyclic voltammograms and (b) Linear sweep voltammograms at a rotating rate of 1600 rpm using different ORR catalysts in the H₂SO₄ (0.5 M) solution. The Co-C-16 catalyst exhibited a negative shift of onset potential by ~70 mV and a decrease of j_{lim} by ~1.7 mA cm⁻² when compared with the Pt/C catalyst.

Table S3. Performance of representative carbon-based catalysts reported recently.^a

Catalyst ^b	E_{onset} (V)	$E_{1/2}$ (V)	j_{lim} (mA cm ⁻²)	Electrolyte	P_{max} in fuel cells	Ref
Co-SAs@NC	~-0.87	0.82	4.96	0.1 M KOH	105.3 mW cm ⁻² in alkaline Zn-air fuel cell	S1
Co-SAs@NC	~-0.75	~-0.68	~4.2	0.1 M KCl	-	S1
Co-SAs@NC	~-0.65	~-0.62	~2.9	0.5 M H ₂ SO ₄	-	S1
Co@N-C-800	~-0.88	0.85	5.1	0.1 M KOH	66 mW cm ⁻² in alkaline Zn-air fuel cell	S2
Co@N-C-800	~-0.67	0.56	~4.2	0.1 M HClO ₄	-	S2
Co@N-CNTF-2	~-0.85	0.81	~4.7	0.1 M KOH	91 mW cm ⁻² in alkaline Zn-air fuel cell	S3
1.6%CoNC-ArNH ₃	~-0.82	0.758	~5.4	0.1 M HClO ₄	800 mW cm ⁻² in proton exchange membrane fuel cell	S4
Ni ₂ Co ₃ @ht-CN	~-0.59	0.51	~6.4	0.5 M KNO ₃	47 mW cm ⁻² in neutral Zn-air fuel cell	S5
Ni ₂ Co ₃ @ht-CN	~-0.88	0.84	~4.6	0.1 M KOH	314 mW cm ⁻² in alkaline Zn-air fuel cell	S5
Co-pyridinic N-C	~-0.93	0.87	~5.3	0.1 M KOH	-	S6
Co-pyridinic N-C	~-0.86	0.84	~4.0	0.5 M H ₂ SO ₄	-	S6
NiFe ₂ O ₄ /FeNi ₂ S ₄ HNSs	~-0.57	~-0.56	~2.26	0.2 M phosphate buffer solution	44.4 mW cm ⁻² in neutral Zn-air fuel cell	S7

^a E_{onset} is defined as the potential at the current density of 1 mA cm⁻². The symbol of ~ represents the estimated value based on the references. P_{max} : the maximum power density.

^b The names of the catalysts were excerpted from the references.

Table S4. Performances of catalysts in various fuel cells.^a

Catalyst	Alkaline Zn-air fuel cell		Neutral Zn-air fuel cell		Direct methanol fuel cell	
	OCV (V)	P_{max} (mW cm ⁻²)	OCV (V)	P_{max} (mW cm ⁻²)	OCV (V)	P_{max} (mW cm ⁻²)
Co-C-0	1.40	70.03	1.37	27.27	0.41	0.20
Co-C-16	1.38	86.42	1.29	35.07	0.39	0.25
Pt/C	1.44	81.77	1.32	30.13	0.53	0.42

^aOCV: open circuit voltage, P_{max} : maximum power density.

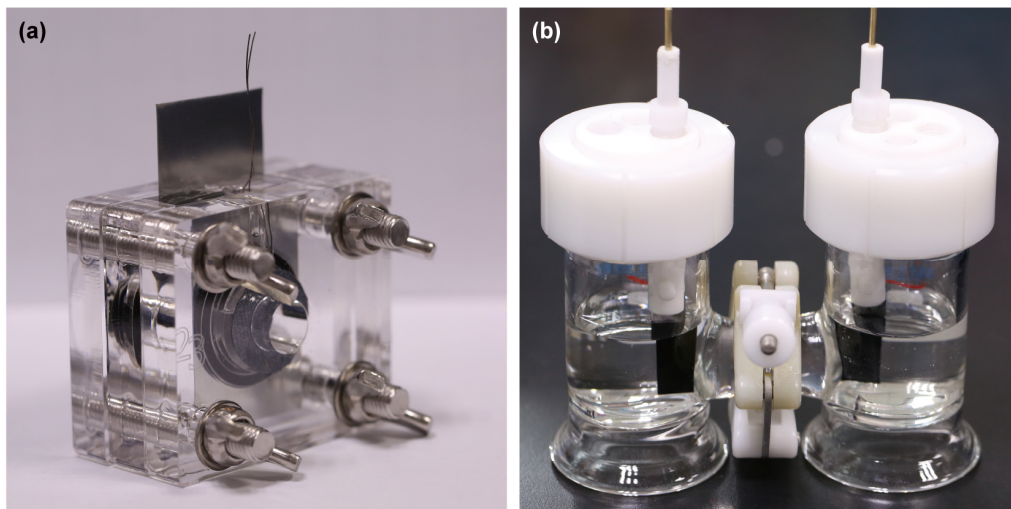


Figure S11. Photos of (a) the Zn-air fuel cell and (b) the direct methanol fuel cell.

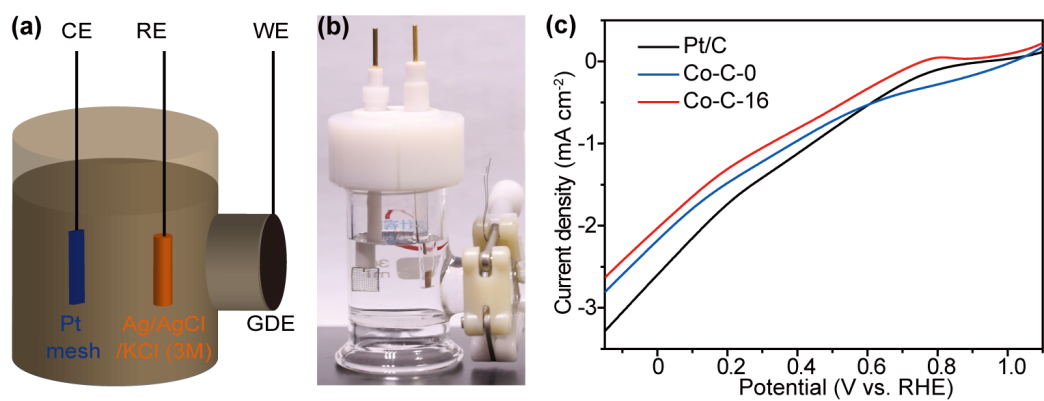


Figure S12. (a) Schematic diagram and (b) photo of the half cell. CE: counter electrode, RE: reference electrode, WE: working electrode, and GDE: gas-diffusion electrode. (c) Polarization curves of half cells using different catalysts.

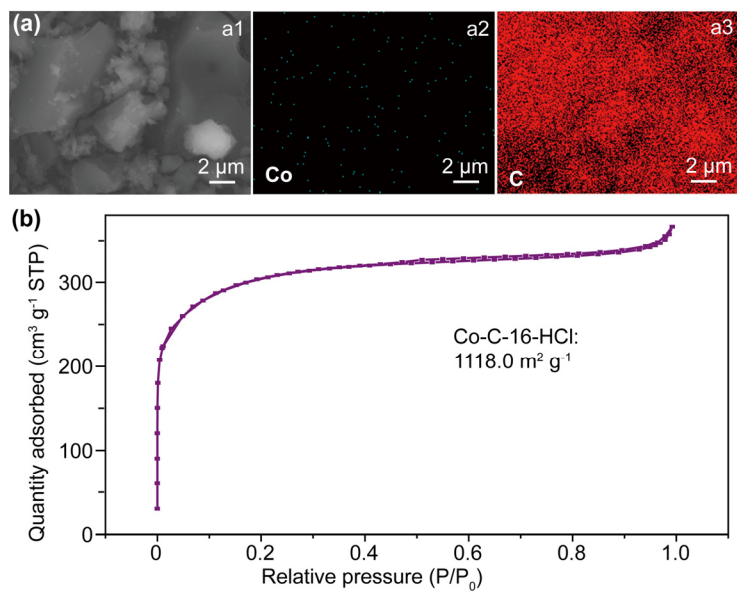


Figure S13. (a) SEM image (a1) and corresponding elemental mapping (a2, a3), and (b) N₂ sorption isotherm of the Co-C-16-HCl.

Reference

- [S1] Han, X.; Ling, X.; Wang, Y.; Ma, T.; Zhong, C.; Hu, W.; Deng, Y. Generation of nanoparticle, atomic-cluster, and single-atom cobalt catalysts from zeolitic imidazole frameworks by spatial isolation and their use in zinc–air batteries. *Angewandte Chemie International Edition* **2019**, *58*, 5359-5364.
- [S2] Kong, F.; Fan, X.; Zhang, X.; Wang, L.; Kong, A.; Shan, Y. Soft-confinement conversion of Co-Salen-organic-frameworks to uniform cobalt nanoparticles embedded within porous carbons as robust trifunctional electrocatalysts. *Carbon* **2019**, *149*, 471-482.
- [S3] Guo, H.; Feng, Q.; Zhu, J.; Xu, J.; Li, Q.; Liu, S.; Xu, K.; Zhang, C.; Liu, T. Cobalt nanoparticle-embedded nitrogen-doped carbon/carbon nanotube frameworks derived from a metal–organic framework for tri-functional ORR, OER and HER electrocatalysis. *Journal of Materials Chemistry A* **2019**, *7*, 3664-3672.
- [S4] Chen, L.; Liu, X.; Zheng, L.; Li, Y.; Guo, X.; Wan, X.; Liu, Q.; Shang, J.; Shui, J. Insights into the role of active site density in the fuel cell performance of Co-N-C catalysts. *Applied Catalysis B: Environmental* **2019**, *256*, 117849.
- [S5] Yu, L.; Yi, Q.; Yang, X.; Chen, Y. An easy synthesis of Ni-Co doped hollow C-N tubular nanocomposites as excellent cathodic catalysts of alkaline and neutral zinc-air batteries. *Science China Materials* **2019**, *62*, 1251-1264.
- [S6] Ha, Y.; Fei, B.; Yan, X.; Xu, H.; Chen, Z.; Shi, L.; Fu, M.; Xu, W.; Wu, R. Atomically dispersed Co-pyridinic N-C for superior oxygen reduction reaction. *Advanced Energy Materials* **2020**, 2002592.
- [S7] An, L.; Zhang, Z.; Feng, J.; Lv, F.; Li, Y.; Wang, R.; Lu, M.; Gupta, R. B.; Xi, P.; Zhang, S. Heterostructure-promoted oxygen electrocatalysis enables rechargeable zinc–air battery with neutral aqueous electrolyte. *Journal of the American Chemical Society*, **2018**, *140*, 17624-17631.